Pentacene Monolayer Trapped between Graphene and Substrate

Qicheng ZHANG[1], Boyu PENG[2], Paddy Kwok Leung Chan[2], Zhengtang LUO[1,*]

[1]Department of Chemical and Biomolecular Engineering, the University of Hong Kong Science and Technology

[2]Department of Mechanical Engineering, the University of Hong Kong

Email: keztluo@ust.hk

ABSTRACT Self-assembled pentacene monolayer can be fabricated between solid-solid interface of few-layer graphene (FLG) and mica substrate, through a diffusion-spreading method. By utilizing a transfer method that allows us to sandwich pentacene between graphene and mica, followed by controlled annealing, we enables the diffused pentacene to be trapped in the interfaces and lead to the formation of a stable monolayer. We found that the formation of monolayer is kinetically favored by using a 2D Ising lattice gas model for pentacene trapped between graphene-substrate interfaces. This kinetic Monte Carlo simulation results indicate that, due to the graphene substrate enclosure, the spreading of the first layer proceeds faster than the second layer, as the kinetics favors the filling of void by molecules from the second layer. This graphene assisted monolayer assembly method provides a new venue for fabrication of two-dimensional monolayer structures.

INTRODUCTION

Due to their exceptional electronic, mechanical and thermal properties, as well as impermeability to gas molecules, graphene materials has attracted tremendous attention in scientific research [1, 2]. Utilizing their exceptional impermeability to molecules, it was shown that a monolayer or few layers of self-assembled water molecules can be trapped between graphene and mica interface [3-6], when placed between these two solid substrates. Similar trapped monolayers are also observed for other molecules, such as organic molecules of tetrahydrofuran [7]. On the other hand, there are also enormous interests in pentacene monolayers for their potential application as high mobility organic thin-film transistor [8], as well as in sensing application [9]. The traditional method to obtain pentacene monolayer is by high vacuum vapor deposition [10], in which the growth of pentacene thin film strongly dependent on the quality of initial few layers [10]. With this method, the control of pentacene monolayer mainly relies on tuning of pentacene diffusion constants, changing the type of substrate material, and controlling substrate temperature [10]. Difficulties in controlling these parameters has resulted in poor film quality and bottlenecked application of pentacene thin films. Moreover, in order to enhance crystal structure, post-treatment such as annealing are required, which lead to limited improvement in crystallinity because of the resulted inevitable desorption of pentacene molecules from out-of-plane direction[11].

In this letter, we demonstrate a graphene-assisted monolayer assemble concept that can be used to trap a pentacene monolayer between graphene and mica substrate, forming a pentacene monolayer. This method takes advantage of the diffusion-spreading kinetics which favors monolayer formation. Here graphene film works as a flat platform for smooth monolayer growth and also provide strong out-of-plane motion constraint which function as a nano-reactor. Our graphene-assisted monolayer trapping method completely eliminates desorption in the annealing process. This method may find application to other aromatic material for fabrication of advanced two-dimensional material such as 2-D polymers [12].

RESULTS AND DISCUSSIONS

We developed the graphene-assisted trapping method inspired by the trapping of water molecule between graphene and mica [13, 14]. Figure 1A illustrates the schematics of the fabrication process. Firstly, two mica substrates are exfoliated and cleaned. Bulk pentacene film of ~ 25 nm thick was deposited on the freshly-cleaved mica substrate by physical vapor deposition. On the second freshly exfoliated mica substrate, few layer graphene (FLG) was deposited using previously established micromechanical exfoliation methods [15]. The graphene/mica substrate is then transferred onto the pentacene/mica following a previously reported procedure [16]. More specifically, the exfoliated FLG/Mica was covered with a layer of PMMA. After that, a carefully carved U-shape PDMS frame was applied to the PMMA/FLG/mica. A droplet of water was added to the edge of mica and immediately immerse in ethanol solution, which lead to the detachment of PDMS/PMMA/FLG film from mica and allow it to float on the ethanol surface. The previously-fabricated pentacene/mica was then used to scoop the PMMA/FLG film from the ethanol surface. After the thermal releasing of PDMS, the PMMA coating was subsequently removed by soaking the material in cold dichloromethane/methanol (1:1, v/v) mixture followed by soaking in cold acetone. The solvents do not dissolve pentacene as confirmed by experiment, while the surface of pentacene may be affected by some of the solvents [17]. The FLG-pentacene-mica sandwich is thus produced (Figure 1B). The prepared structure was then annealed in inert gas atmosphere, with trace amount of hydrogen added to remove residual oxygen.

AFM images of the regions in the vicinity of FLG edges on the mica substrates are depicted in Figure 1B and 1C (with corresponding zoomed images in 1D). As demonstrated in Figure 1C and 1D, after annealing, bulk pentacene at the graphene edges flattens into thin uniform area about 2 μm in size, while regions away from the graphene edges remain in its original heights (Figure 1D). In the meantime, the pentacene not covered by FLG re-evaporated from the substrate, leaving bare mica substrate with traces of adhesive residue. Besides, the annealing process has introduced a significant amount of wrinkles in the graphene, due to the different thermal expansion coefficient of graphene and the substrate [18-20]. Such effects become increasingly severe as the layer number decrease, especially for monolayer. To avoid the complication in morphological study due to wrinkles, here we study morphology of FLG with layer number > 15 only, where the bending strength is one order higher than monolayer graphene [21]. The height of the gap between graphene and mica is ~ 1.5 nm (Figure 1E, where the original graphene thickness, determined prior to deposition, is deduct from the total heights), consistent with the 1.5 nm length of pentacene monolayer as observed in thin-film phase or Campbell phase [22-24].

The existence of pentacene monolayer is further confirmed by Raman spectroscopy. Characteristic peaks around 1156 cm^{-1} and 1178 cm^{-1} (Figure 2A) correspond to C-H in-plane bending modes in pentacene layers [25]. The shoulder peak around 1155 cm^{-1} and 1160 cm^{-1} of bulk pentacene disappears along with red shift of the peak around 1152 cm^{-1}, indicating the formation of monolayer pentacene [26]. For the Raman spectra of graphene in these region, we have seen that the G peak of monolayer pentacene supported graphene red-shifted from 1580 cm^{-1} of pristine graphene , in the same direction of the shift of bulk pentacene supported graphene, further evidencing the formation pentacene layer as the tensile strain of graphene is greatly relaxed when the soft pentacene layer in between serving as a buffer layer during annealing [27]. This is in contrast to the 2D peak, which stays at 2710 cm^{-1} , where the tensile stress relaxation is offset by the competing effects of p-doping shielding [28].

The formation of pentacene monolayer is further confirmed by investigating the topographic features after annealing of the obtained structure for extended period. With annealing at temperature up to 200 °C for 1 hour, dips in strip shape are formed on the graphene terrace (Figure 3A). The progressive widen of dip strip in pentacene monolayer is also observed upon annealing at lower temperature (lowered from 200 °C to 150 °C). Figure 3B depicts AFM images of graphene/pentacene/mica after annealing at 150 °C. The heights of those dips are around ~ 1.5 nm, exactly matches with the height of extended pentacene monolayer (Figure 3C). The dip strips developed and widened from 40 nm to 50 nm (Figure 3D), with shape development pattern similar to conventional viscous fingers, shown in Figure 3E [29-32]. Simultaneously, the overall area of the dip strips shrinks (Figure 3E), indicating a refilling of pentacene molecules from bulk islands to monolayer region.

The formation of pentacene monolayer is resulted from a thin film spreading mechanism. Diffusion-controlled thin layer spreading of small molecules are widely observed experimentally [33-36] and is believed to be kinetically controlled. As can be cleared later, under such mechanism, when pentacene evaporates at appropriate temperature, diffusion-controlled thin layer spreading allows the growth of the first layer from bulk pentacene is fast enough to keep the presence of a monolayer as opposed to the bilayer (or more layers) structure. Figure 4A illustrates the spreading of pentacene from bulk to the mica-graphene interface. This is similar to monolayer thick film spreading of solid-on-solid system [37, 38]. Here we simulated the diffusion-spreading process by kinetic Monte Carlo (kMC) simulation of associated two-dimensional driven Ising lattice gas model [39]. With slight modification, we reconstructed the model as described below. For simplicity, spreading of two layers (indicated by $z = 1$, and $z = 2$ for first and second layer, respectively) is discussed, which reduces heavy calculation power needed starting from experimentally used pentacene thickness and keeps the main spreading features [39]. The first layer is that near the mica substrate (*i.e.* $z = 1$) and the second layer is that near the cover graphene (*i.e.* $z = 2$). At each site $\boldsymbol{r}(x, y, z)$, we assign an occupation number of 0 or 1, standing for void or molecule, respectively. The Hamiltonian of the whole system is slightly modified from the literature [39, 40], as shown in equation 1.

$$\mathcal{H} = -J_{in} \sum_{\substack{|\boldsymbol{r}-\boldsymbol{s}|=1,\\ z(\boldsymbol{r})=z(\boldsymbol{s})}} n(\boldsymbol{r},t)n(\boldsymbol{s},t) - J_{out} \sum_{\substack{|\boldsymbol{r}-\boldsymbol{s}|=1,\\ x(\boldsymbol{r})=x(\boldsymbol{s}),\\ y(\boldsymbol{r})=y(\boldsymbol{s})}} n(\boldsymbol{r},t)n(\boldsymbol{s},t) - A_{sub} \sum_{z=1,2} \frac{n(\boldsymbol{r},t)}{z^3} - A_{cover} \sum_{z=1,2} \frac{n(\boldsymbol{r},t)}{(3-z)^3} - A_{inter} \sum_{\boldsymbol{r}} \left(1 - n(\boldsymbol{r},t)\right) \tag{1}$$

Here, J_{in} and J_{out} represent the nearest-neighbor binding energy for in-plane interaction and out-of-plane interaction, respectively. Interfacial interactions are described by terms A_{sub}, A_{cover} and A_{inter}, representing the interfacial energy between pentacene and mica substrate (A_{sub}), between pentacene and graphene cover (A_{cover}), and between graphene cover and mica substrate (A_{inter}), respectively. Numerical values of those parameters are demonstrated in the supplementary information. At initial state, we set $n(\boldsymbol{r}, 0) = 1$ for $x = 1$ and $n(\boldsymbol{r}, t) = 0$ for $x > 1$ [39]. Mimicking the fast relaxation at the edge connecting bulk reservoir to the spread film, once particle at $x = 1$ moved out, another particle would fill in immediately. Periodical boundary is applied to the y-direction and molecules are assumed to escape from the maximum x edge. By introducing graphene cover, pentacene evaporation from the out-of-plane direction is neglected. For the current simulation there should be no difference between monolayer graphene and FLG.

The simulated results are summarized in Figure 4. Figure 4B illustrates snapshot of spreading of pentacene molecules at 200 °C. We can clearly see from Figure 4D that the spreading of the first layer is much faster than the second layer. A closer inspect into the film reveals that the spread film is not compact but with many voids. However, when lower annealing temperature were used, *i.e.* at 150 °C, we can see that many voids are filled (red circle in Figure 4C) and those patched dips were smoothed into wider stripes (front of the first layer in Figure 4C) and some were diminished, exactly matching with the experimentally observed morphology change shown in Figure 3E. Figure 4D plotted the spreading front position, of the first and second layer respectively, as a function of spreading time. Here the position of front can be calculated by fitting the occupancy at specific x position to an error function. We can clearly see that the first layer spreads significantly faster than the second layer. As indicated by the arrows in Figure 4D, after certain time, the growth of the second layer level off while the first layer keeps growing. In other words, the formation of monolayer is dominant as opposed to the formation of double layer. Our result here is consistent with previous hypothesis that the growth of the firstly is a direct result of filling of the voids of the first layer by molecules in the second layer [39], and reveal itself as faster growth of the first layer.

The existence of an impermeable graphene film renders the spreading of molecular very different from traditional method, where no cover film was applied. As shown in Equation 1, in this diffusion-spreading mechanism, two important parameters dominate in this process, *i.e.* the sublimation/evaporation rate, characterized by J/k_BT, and the ability for molecules to "wet" the substrate, characterized by A/J, where J represents the intermolecular interaction for spreading species and A represents the attraction between spreading species and the substrate. For traditional model, because of the absence of cover layer to protect the spreading species from out-of-plane evaporation, $J/$

$k_B T$ needs to be large enough to prevent such molecular lose. As a result, "complete wetting", due to relatively large interaction between spreading species and the substrate surface is usually required. For example, $J/k_B T = 3$ and $A/J = 10$ is used in some previous report [39]. But the impermeable graphene cover mitigates such requirements. Molecular species with a significant lower value for those two parameters, such as pentacene/mica case in which $J/k_B T = J_{in}/k_B T = 0.817$ and $A/J = (A_s + A_c - A_{sc})/J_{inter} = 3.14$, are observed to form ordered thin film. In other words, the existence of a graphene cover allows molecules with small $J/k_B T$ value to diffuse along with that of voids, unlike the case for high $J/k_B T$ value, where molecule diffusion is limited due to the low volatility of molecules. Furthermore, the rate of voids filling is also decreased for smaller A/J values, as A characterize the energy gain, while J are related to energy penalty. Consequently traditional simulation of film spreading demonstrates that the evolution of the front position ($x(t)$) relates to the growth time as $x(t) \sim t^{\frac{1}{2}}$ where t is the growth time [39]. However, this relationship is not maintained in our case, where the $t^{\frac{1}{2}}$ relationship is no longer applicable.

Our model provides good explanation to the monolayer formation along with the morphology change upon low temperature annealing. We also note that the energy penalty from molecule friction was not taking into account which has considerable effect on molecule diffusion. Such contribution could have impact on the stripe pattern formed at graphene-silica interface (Figure S2). We are on our way to study this further.

CONCLUSION

In conclusion, we demonstrate the fabrication of pentacene monolayer by a graphene-assisted trapping method. We have shown that the formation of monolayer is kinetically favorable with graphene enclosure, as demonstrated in the kinetic Monte Carlo simulation. When sandwiched between graphene and substrate, the growth rate the pentacene monolayer is significantly faster than the second layer as the void in the first layer is filled by the molecules from the second layer, which consequently lead the expansion of monolayer at the expense of thicker layers. Such a method opens new venue for growing monolayer with low cohesive energy, which would otherwise impossible to form monolayer structure. It may be suitable to be applied to other material with moderate interaction with graphene/mica or other inert surfaces.

AKNOWLEDGEMENT

This project is supported by the Research Grant Council of Hong Kong SAR (Project number 623512 and DAG12EG05) and SFC/RGC Joint Research Scheme (Project number X-HKUST603/14). Technical assistance from the Materials Characterization and Preparation Facilities is greatly appreciated.

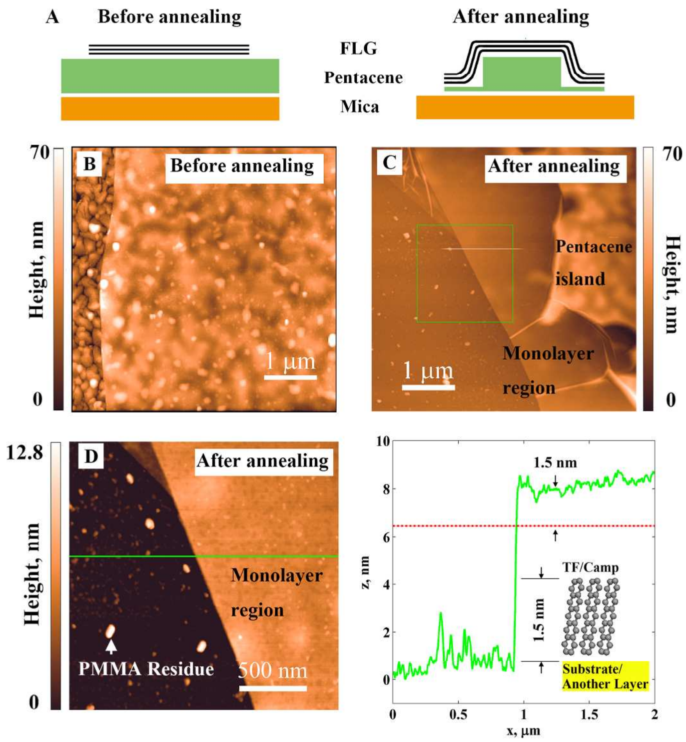

Figure 1 Graphene-assisted trapping method. A) The pentacene coated substrate (mica) is first covered by few layer graphite (FLG) flakes (left) followed by thermal annealing. The monolayer is created when the pentacene near the edge of FLG flakes has been evaporated, forcing the pentacene to spread through the mica-FLG interface (right). **B)** The same FLG flake before forming the FLG-pentacene-mica sandwich. **C)** The AFM image displays that monolayer pentacene formed at the FLG cover edge. **D)** The zoomed-in view of the box in C). On the mica surface without FLG, pentacene evaporated and some PMMA residue remains as indicated by the arrow. **E)** The AFM profile demonstrates that the height difference of the same FLG flake before and after pentacene monolayer formation is 1.5 nm, fitting one monolayer height of pentacene of thin film or Campbell phase. The red dash-dot line indicates the FLG thickness (details shown in Figure S1) and green solid line indicates the line in D).

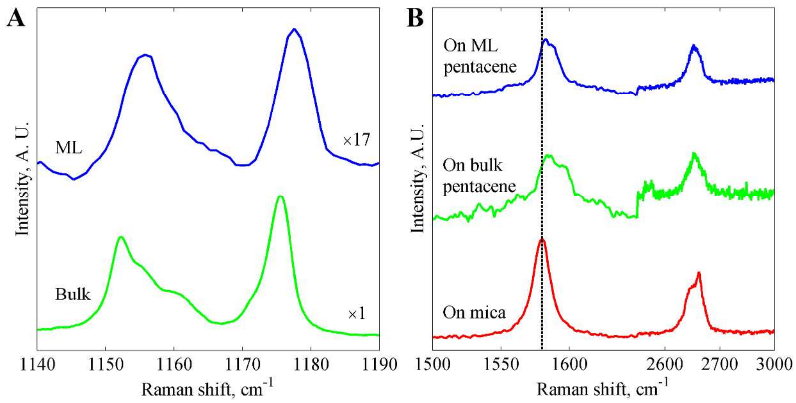

Figure 2 Raman spectra. **A)** The two characteristic peaks at 1100 cm^{-1} to 1200 cm^{-1} demonstrate the presence of pentacene thin film. The shoulder peak around 1155 cm^{-1} and 1160 cm^{-1} of bulk pentacene disappears along with red shift of the peak around 1152 cm^{-1}, indicating the formation of monolayer pentacene. The 633 nm excitation wavelength is used to achieve resonant enhancement. **B)** The micro Raman signal for the graphene flakes only (bottom red line), FLG covered bulk pentacene (middle green line) and FLG covered monolayer pentacene (top blue line) demonstrate that the trapped pentacene slightly shifts the G peak to the right. The excitation wavelength is 514 nm.

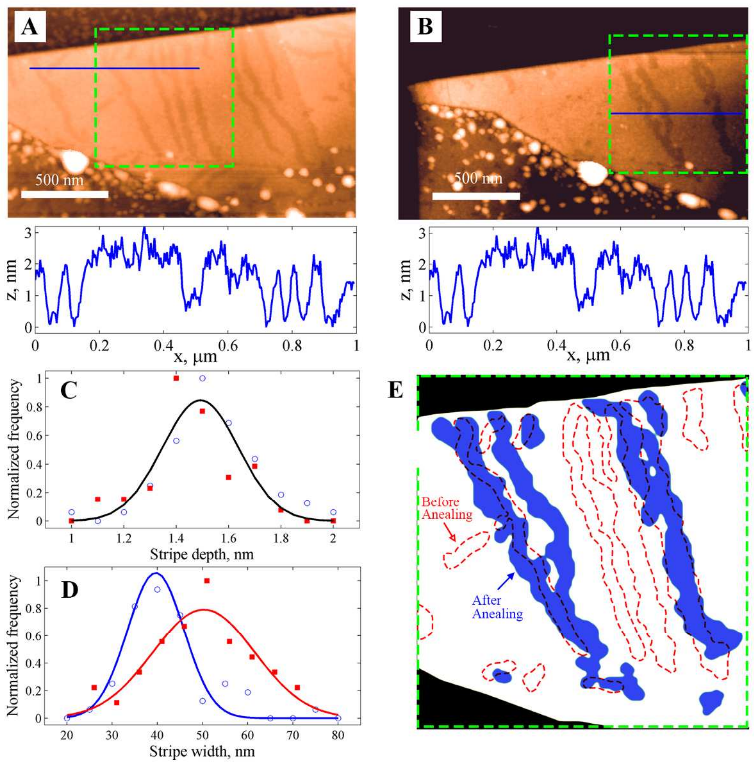

Figure 3 Dynamic pentacene spreading process at sub-monolayer coverage. **A)** The dip strip pattern before 150 °C annealing. The dip strip profile is indicated by the blue line. **B)** AFM image of the same sample demonstrates that the dip strips rearrange upon annealing at 150 °C for 1 hr. The strip profile is indicated in lower panel. **C)** The dip strips in both A) (blue hollow circles) and B) (red solid squares) have similar depths measured by AFM. The measured depths undulate around a Gaussian curve with mean at 1.5 nm. **D)** The mean strip width increases from 40 nm of A) to 50 nm of B). The widths are measure at the inflection points of the strip profile. **E)** The morphology change of the dip strips indicated in the green dash line boxes of A) and B) assimilates that of river evolution. The red dash-line delineated area evolved to the blue filled area after 150 °C annealing.

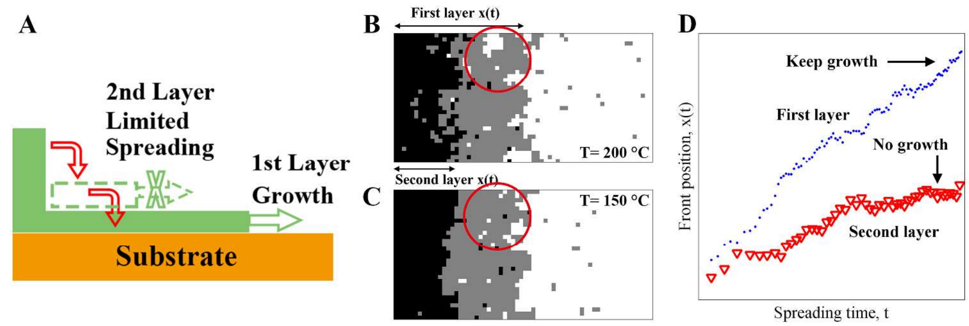

Figure 4 Kinetic Monte Carlo (kMC) simulation of Ising lattice gas model. **A)** The spreading kinetics allows the first layer to grow while limiting the growth of second layer. The dash red arrows indicate the pentacene mass transport direction. Here, the graphene cover is not shown for simplicity. **B)** One of the spreading frames at high temperature (200 °C), the graphene-mica interface is indicated with white color, the first layer gray color and the second layer black color. **C)** Annealing starting from B) at 150 °C for certain time resulted in more compact film with smoother edges. As demonstrated in the curing of void in the red circle and the second layer. **D)** The front position evolution with time for both the first layer and the second layer. The growth rate of the first layer keeps increase while the growth of the second layer level off as indicated by the arrows.

References

1. Novoselov, K.S., et al., *Electric field in atomically thin carbon films.* Science, 2004. **306**(5696): p. 666-669.
2. Berry, V., *Impermeability of graphene and its applications.* Carbon, 2013. **62**(0): p. 1-10.
3. He, K.T., et al., *Scanning tunneling microscopy study and nanomanipulation of graphene-coated water on mica.* Nano Letters, 2012. **12**(6): p. 2665-2672.
4. Xu, K., P. Cao, and J.R. Heath, *Graphene visualizes the first water adlayers on mica at ambient conditions.* Science, 2010. **329**(5996): p. 1188-1191.
5. Severin, N., et al., *Reversible Dewetting of a Molecularly Thin Fluid Water Film in a Soft Graphene–Mica Slit Pore.* Nano Letters, 2012. **12**(2): p. 774-779.
6. Rezania, B., et al., *Influence of graphene exfoliation on the properties of water-containing adlayers visualized by graphenes and scanning force microscopy.* Journal of Colloid and Interface Science, 2013. **407**: p. 500-504.
7. Cao, P., et al., *Atomic force microscopy characterization of room-temperature adlayers of small organic molecules through graphene templating.* Journal of the American Chemical Society, 2011. **133**(8): p. 2334-2337.
8. Gundlach, D.J., et al., *Pentacene organic thin-film transistors - Molecular ordering and mobility.* IEEE Electron Device Letters, 1997. **18**(3): p. 87-89.
9. Mirza, M., et al., *Novel Top-Contact Monolayer Pentacene-Based Thin-Film Transistor for Ammonia Gas Detection.* ACS Applied Materials & Interfaces, 2014. **6**(8): p. 5679-5684.
10. Ruiz, R., et al., *Pentacene thin film growth.* Chemistry of Materials, 2004. **16**(23): p. 4497-4508.
11. Guo, D., et al., *Effect of annealing on the mobility and morphology of thermally activated pentacene thin film transistors.* Journal of Applied Physics, 2006. **99**(9) : p. 094502.
12. Colson, J.W. and W.R. Dichtel, *Rationally synthesized two-dimensional polymers.* Nat Chem, 2013. **5**(6): p. 453-465.
13. Shim, J., et al., *Water-gated charge doping of graphene induced by mica substrates.* Nano Lett, 2012. **12**(2): p. 648-54.
14. Ochedowski, O., B.K. Bussmann, and M. Schleberger, *Graphene on mica - intercalated water trapped for life.* Sci Rep, 2014. **4**: p. 6003.
15. Novoselov, K.S., et al., *Two-dimensional atomic crystals.* Proceedings of the National Academy of Sciences of the United States of America, 2005. **102**(30): p. 10451-10453.
16. Li, H., et al., *A Universal, Rapid Method for Clean Transfer of Nanostructures onto Various Substrates.* ACS nano, 2014. **8**(7): p. 6563-6570.
17. Gundlach, D.J., et al., *Solvent-induced phase transition in thermally evaporated pentacene films.* Applied Physics Letters, 1999. **74**(22): p. 3302-3304.
18. Bao, W.Z., et al., *Controlled ripple texturing of suspended graphene and ultrathin graphite membranes.* Nature Nanotechnology, 2009. **4**(9): p. 562-566.
19. Levy, N., et al., *Strain-induced pseudo-magnetic fields greater than 300 tesla in graphene nanobubbles.* Science, 2010. **329**(5991): p. 544-547.
20. Ryu, S., et al., *Atmospheric Oxygen Binding and Hole Doping in Deformed Graphene on a SiO2 Substrate.* Nano Letters, 2010. **10**(12): p. 4944-4951.
21. Poot, M. and H.S.J. van der Zant, *Nanomechanical properties of few-layer graphene membranes.* Applied Physics Letters, 2008. **92**(6): p. 063111.
22. Chhikara, M., et al., *Pentacene on graphene: Differences between single layer and bilayer.* Carbon, 2014. **69**: p. 162-168.
23. Chhikara, M., et al., *Effect of Water Layer at the SiO2/Graphene Interface on Pentacene Morphology.* Langmuir, 2014. **30**(39): p. 11681-11688.

24. Götzen, J., et al., *Growth and structure of pentacene films on graphite: Weak adhesion as a key for epitaxial film growth.* Physical Review B - Condensed Matter and Materials Physics, 2010. **81**(8) : p. 085440.
25. He, R., et al., *Resonant Raman scattering in nanoscale pentacene films.* Applied Physics Letters, 2004. **84**(6): p. 987-989.
26. He, R., et al., *Low-lying lattice modes of highly uniform pentacene monolayers.* Applied Physics Letters, 2009. **94**(22) : p. 223310.
27. Huang, M., et al., *Phonon softening and crystallographic orientation of strained graphene studied by Raman spectroscopy.* Proc Natl Acad Sci U S A, 2009. **106**(18): p. 7304-8.
28. Das, A., et al., *Monitoring dopants by Raman scattering in an electrochemically top-gated graphene transistor.* Nat Nanotechnol, 2008. **3**(4): p. 210-5.
29. Arnéodo, A., et al., *Uncovering the analytical Saffman-Taylor finger in unstable viscous fingering and diffusion-limited aggregation.* Physical Review Letters, 1989. **63**(9): p. 984-987.
30. Pelcé, P., *Dynamics of curved fronts*. 1988, Boston: Academic Press.
31. Tanveer, S., *Analytic theory for the selection of a symmetric Saffman–Taylor finger in a Hele–Shaw cell.* Physics of Fluids (1958-1988), 1987. **30**(6): p. 1589-1605.
32. Taylor, G. and P.G. Saffman, *A Note on the Motion of Bubbles in a Hele-Shaw Cell and Porous Medium.* The Quarterly Journal of Mechanics and Applied Mathematics, 1959. **12**(3): p. 265-279.
33. Ispolatov, I. and B. Widom, *Unified approach to prewetting and wetting phase transitions.* Physica A, 2000. **279**(1-4): p. 203-212.
34. Leger, L., et al., *Precursor Film Profiles of Spreading Liquid-Drops.* Physical Review Letters, 1988. **60**(23): p. 2390-2393.
35. Churaev, N.V., *Wetting Films and Wetting.* Revue De Physique Appliquee, 1988. **23**(6): p. 975-987.
36. Radigan, W., et al., *Kinetics of spreading of glass on fernico metal.* Journal of Colloid and Interface Science, 1974. **49**(2): p. 241-248.
37. Humfeld, K.D., S. Garoff, and P. Wynblattt, *Analysis of pseudopartial and partial wetting of various substrates by lead.* Langmuir, 2004. **20**(7): p. 2726-2729.
38. Prevot, G., et al., *Macroscopic and mesoscopic surface diffusion from a deposit formed by a Stranski-Krastanov type of growth: Pb on Cu(100) at above one layer of coverage.* Physical Review B, 2000. **61**(15): p. 10393-10403.
39. Abraham, D.B., R. Cuerno, and E. Moro, *Microscopic model for thin film spreading.* Physical Review Letters, 2002. **88**(20): p. 206101-1.
40. Lukkarinen, A., K. Kaski, and D.B. Abraham, *Mechanisms of Fluid Spreading - Ising Model Simulations.* Physical Review E, 1995. **51**(3): p. 2199-2202.